

Integrating ambient noise with GIS for a new perspective on volcano imaging and monitoring: the case study of Mt. Etna

Guardo R.^{a,*}, De Siena L.^{b,1}

^a*Instituto de Investigación en Paleobiología y Geología (CONICET-UNRN), Av. J.A. Roca 1242, (8332) General Roca, Río Negro, Argentina*

^b*University of Aberdeen, School of Geosciences, Dept. Geology and Petroleum Geology, Meston Building, King's College, Aberdeen AB24 3UE Scotland, UK.*

Abstract

The timely estimation of short- and long-term volcanic hazard relies on the **availability** of detailed 3D geophysical images of volcanic structures. High-resolution seismic models of the absorbing uppermost conduit systems and highly-heterogeneous shallowest volcanic layers, while particularly challenging to obtain, provide important data to locate feasible eruptive centers and forecast flank collapses and lava ascending paths. Here, we model the volcanic structures of Mt. Etna (Sicily, Italy) and its outskirts using the Horizontal to Vertical Spectral Ratio method, generally applied to industrial and engineering settings. The integration of this technique with Web-based Geographic Information System improves precision during the acquisition phase. It also integrates geological and geophysical visualization of 3D surface and subsurface structures in a queryable environment representing their exact three-dimensional geographic position, enhancing interpretation. The results show high-resolution 3D images of the shallowest volcanic and feeding systems, which complement (1) deeper seismic tomography imaging and (2) the results of recent remote sensing imaging. The study recovers a vertical structure that divides the pre-existing volcanic complexes of Ellittico and Cuvigghiuni. This could be interpreted as a transitional phase between the two systems. A comparison with recent remote sensing and geological results, however, shows that anomalies are generally related to volcano-tectonic structures active during the last 17 years. We infer that seismic noise measurements from miniaturized instruments, when combined with remote sensing techniques, represent an important resource to monitor volcanoes in unrest,

reducing the risk of loss of human lives and instrumentation.

Keywords: Etna, Seismic Imaging, Volcano Imaging, Instrumental developments, GIS-based system, HVSR

1. Introduction

Mt. Etna volcano (Sicily, Italy) is the highest volcano of the Eurasian plate (3343m a.s.l.) and one of the most active in the world. Due to its persistent eruptive activity throughout the last century and its proximity to highly urbanized areas, it is highly hazardous and thus well monitored. Understanding its dynamics and imaging its shallow subsurface structures is considered a crucial step to be taken in order to develop an effective eruption-forecasting model and devise efficient responses to unexpected changes in its volcanological behaviour [Del Negro et al., 2013]. Geophysical measurements and derived tomographic models contribute to the assessment of the physical state, shape, and dimension of feeding systems in volcanoes. Seismic ray-dependent travel-time and attenuation tomography generate 3D images of the inner structures of a volcano, and are increasingly becoming a standard imaging and monitoring tool [Lees and Lindley, 1994; De Gori et al., 1999; Patanè et al., 2006a; De Siena et al., 2010; Koulakov et al., 2010; Koulakov, 2013]. At Mt. Etna, the first regional-scale travel-time and high-frequency attenuation imaging dates back to 1980 [Sharp et al., 1980]. This was followed by local travel-time 3D velocity studies focused on imaging depths down to 20 km under the central portion of the volcano [Hirn et al., 1991; Cardaci et al., 1993; De Luca et al., 1997]. Seismic images have steadily improved resolution on structures in the shallow part of the Earth [Patanè et al., 2002, 2003; De Gori et al., 1999; Patanè et al., 2006a; Alparone et al., 2012], in an attempt to monitor magma intrusions with time-resolved models [Patanè et al., 2006a]. As of today, however, imaging of the volcanic cone is limited above 1 km a.s.l, with a resolution of 1 km [Alparone et al., 2012].

*Corresponding author

Email addresses: rguardo@unrn.edu.ar (Guardo R.), lucadesiena@abdn.ac.uk (De Siena L.)

¹<http://www.abdn.ac.uk/geosciences/people/profiles/lucadesiena>

22 It is challenging to obtain high-resolution seismic images of a volcanic edifice. Seismic
23 methods based on coherent-wave propagation are affected by site effects, highly-reflective
24 topography, and complex 3D propagation effects. These corrupt both seismic phases and
25 amplitudes, which are better described by stochastic models and resonance [Neuberg and
26 Pointer, 2000; Wegler, 2003; De Siena et al., 2014, 2016]. A full 3D imaging of these Earth
27 layers is hindered by the lack of a dense seismic network, with node spacing of the order of
28 e. g. 250 m [Kiser et al., 2016]; this lack is due to the elevated economic costs, installation
29 difficulty, high level of risk for operators when installing standard seismic stations, and
30 has been used as a valid argument for the development of alternative geophysical imaging
31 techniques in volcanoes [Carbone et al., 2014].

32 In this study, we try to close the gap between deep travel-time tomography imaging, sur-
33 face geomorphology information, and shallow feeding systems modelling, using the Horizon-
34 tal to Vertical Spectral Ratio (HVSR) method integrated with the Geographic Information
35 System (GIS). The HVSR technique uses seismic ambient noise data recorded at a single
36 station and has been developed in the framework of civil engineering to study resonance fre-
37 quencies of buildings [Nakamura, 1989; Parolai et al., 2002]. The method has already been
38 used in Earth subsurface imaging, with applications spanning from the characterization of
39 thermal basins [Galgaro et al., 2014] to the study of lateral heterogeneity in small alluvial
40 valleys [Chávez-García and Kang, 2014]. Surface waves (the main constituents of ambient
41 noise) can reveal novel information about the structure of the volcanic edifice [Neuberg and
42 Pointer, 2000]. The method may thus represent the right complement to passive tomo-
43 graphic imaging, providing shallow geological information. Still, in volcanoes, the HVSR
44 is generally used to measure seismic site effects only [Mora et al., 2001]. Almendros et al.
45 [2004] improve the HVSR method and apply it at Teide volcano. The authors estimate a
46 time-dependent HVSR and create vibration frequencies maps across the summit area of the
47 volcano. Merging their HVSR results with different methodologies and geological constraints
48 they achieve an adequate interpretation of the shallow subsurface volcanic structures.

49 Remote sensing is an important alternative to seismic imaging when investigating the
50 shallowest volcanic crust. Using **DInSAR** and GPS data to study ground deformation, it

51 was possible to locate in space and time the position of the dike that produced the 2008
52 eruption of Mt. Etna [Currenti et al., 2011]. Using GIS in combination with the HVSR
53 method opens a path (1) to see beyond the shape and dimensions of the structures, for an
54 improved correlation with geomorphological information; (2) to locate anomalies in space
55 exactly and perform query to measure relevant quantities like volume, size, and extension
56 of the anomalies [Barreca et al., 2013]; (3) to precisely overlap any kind of map (thermal,
57 tectonic, geological, tomographic, etc.), constraining the interpretation of the seismological
58 results [De Siena et al., 2016]. Mount Etna is one of the most studied volcanoes in the
59 world, thus the perfect laboratory to test new methods to image the uppermost part of
60 volcanic cones, with the aim of better predicting future shallow magma ascending path.
61 The experiment of joint seismic and GIS data acquisition as well as the feasible automation
62 of data collection and analysis via the development of smaller instrumentation [Middlemiss
63 et al., 2016] will then represent a feasible resource for hazard assessment solution during
64 volcanic crises.

65 2. Geological and structural background

66 Mount Etna volcano is considered a relatively young volcano with a developing process
67 started about 500 ka ago, in the Quaternary. The volcano is divided into 4 supersynthems
68 and 8 synthems, according to the isotopic datation of De Beni et al. [2011]. The actual
69 shape of the volcano is the result of the last synthem (“Il Piano synthem”), begun around
70 10.4 ka ago. It has an extension of 47 km from North to South and 38 km from East to
71 West and an area of about 1200 km².

72 The volcano is located at the boundary between the Calabro–Peloritan Arc (North)
73 and the Hyblean foreland (South) [Branca et al., 2004; Lentini, 1982; Gillot et al., 1994].
74 On the eastern shore of Etna (and Sicily) there is the “Malta–Hyblean escarpment”, an
75 important system of faults that extends uninterrupted from Malta to the Aeolian Islands
76 passing through the Hyblean area (Fig. 1).

77 The Maltese–Hyblean–Aeolian faults system is considered the main discontinuity be-
78 tween the African plate (**West**) and the Ionian oceanic microplate (**East**) [Gvirtzman and

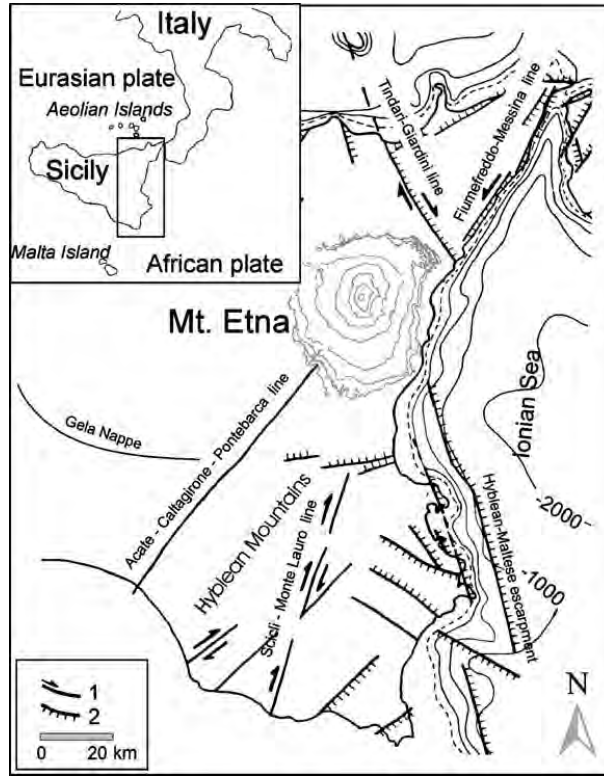


Figure 1: Geological-structural sketch of eastern Sicily from Patanè et al. [2006b]. The legend in the lower left panels marks with (1) the main tectonic lines and (2) the main faults. The Etnean area and its topography are highlighted using contour lines.

79 Nur, 1999] as well as the major contributor to the volcano feeding system through an as-
 80 thenospheric window [Lanzafame and Bousquet, 1997]. The western sector, named by Patanè
 81 et al. [2006b] “Domain a” (Fig. 2), is characterized by faults and fractures with a prevalent
 82 NE-SW direction. The intersection of “Domain a”, comprising NE-SW-oriented structures,
 83 and “Domain b” (Fig. 2), comprising NW-SE-oriented structures, creates discontinuities
 84 that are considered the main cause of magma uprising to the main craters [Patanè et al.,
 85 2006b].

86 3. Instruments and Data

87 In this study, we combine geophysical techniques with information and communication
 88 technologies (ICT) and remote sensing. Seismic data were recorded by a single seismic

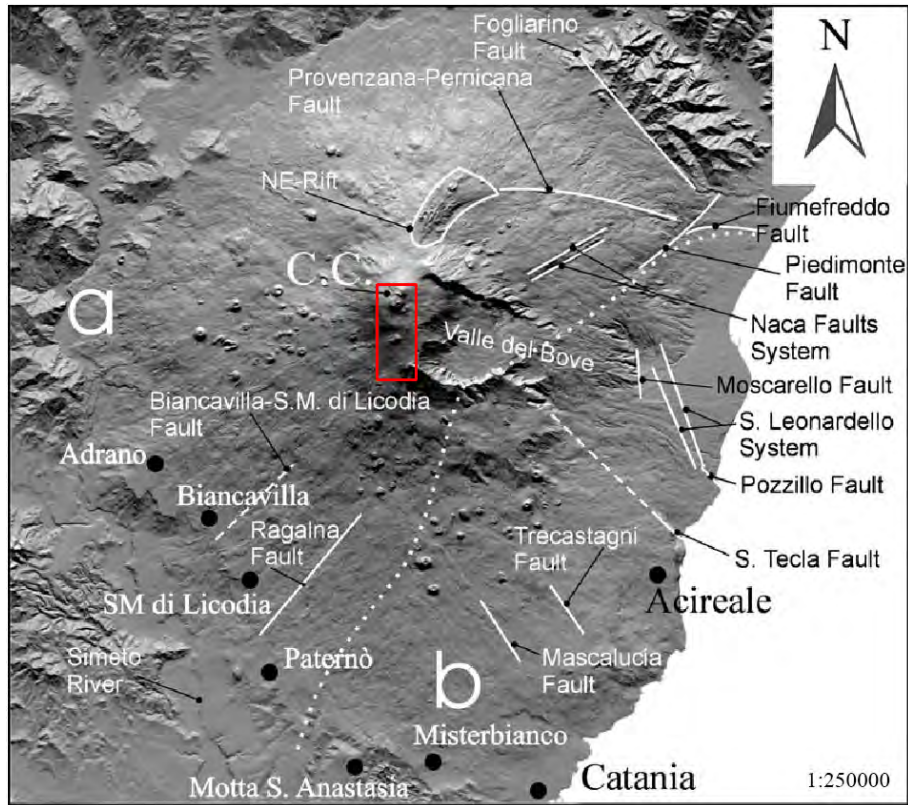


Figure 2: Structural framework of Mount Etna from Patanè et al. [2006b]. Domain “a” is characterized by structures with a prevalent NE-SW orientation. In the domain “b” the NW-SE and NNW-SSE structures are predominant. The two areas are separated by a white dotted line. The red rectangle outlines our study area.

89 station, which was moved in space in order to apply the HVSR technique. As ICT and
 90 remote sensing, we used a GIS environment, a tablet PC, and a GPS antenna. The first
 91 phase of the study has been the creation of the workspace inside the GIS environment. In
 92 the second phase, we acquired field data. Finally, data have been elaborated in a joint
 93 geophysics and GIS environment.

94 3.1. GIS and WEBGIS

95 The setup of a workspace implementing a reliable coordinate system and including all
 96 available data from literature is a fundamental step to develop an accurate field work [Barreca
 97 et al., 2013]. We chose an area of 10.5 km² located between 14.98 and 15.00 longitude E and

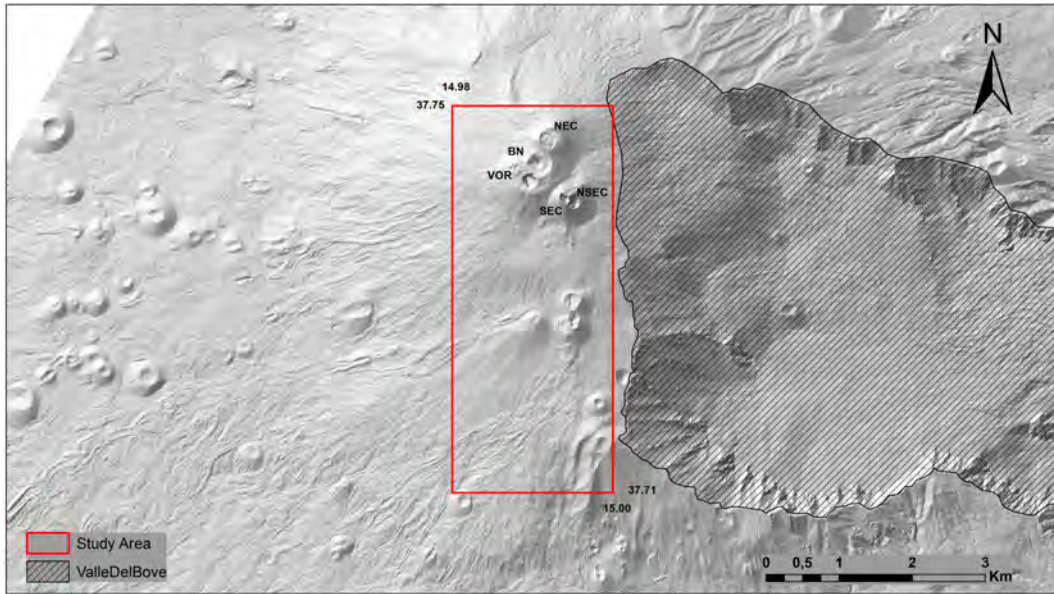


Figure 3: Digital Elevation Model of Mt. Etna as basemap. The main craters are indicated (VOR, Voragine; BN, Bocca Nuova; NEC, NE Crater; SEC, SE Crater; NSEC, New SE Crater).

98 37.71 and 37.75 latitude N, spanning altitudes between 2281 m and 3265 m a.s.l. (Fig. 3).

99 The area was subsequently subdivided into 22 W-E oriented lines and 9 S-N oriented
 100 lines, with nodes spaced 250 m, giving an array of 21 rows and 8 columns. The intersections
 101 of these lines form 198 points. 37 of these points were cut off, due either to their proximity
 102 to the craters or to the time restrictions during acquisition, thus performed at a total of 161
 103 points (Fig. 4).

104 To allow us to be more accurate on reaching the measurement points we
 105 created, for each point, 3 buffer circles at 5, 10 and 15 meters, respectively. Two basemaps
 106 were added to the workspace as final step of the set up: a digital elevation model (DEM) of
 107 Mount Etna and a topographic map with a scale 1:10000 [Bisson et al., 2016]. The workspace
 108 was then uploaded to a server in order to obtain a WebGIS, which is a combination of the
 109 WEB standards with geographic information system [Fu and Sun, 2010]. Hence, we were
 110 able to use this online map operating on a portable device (tablet PC) and carry it to every
 111 measurement point. Due to the risk of losing connectivity, the map was also downloaded
 112 into the tablet local storage.

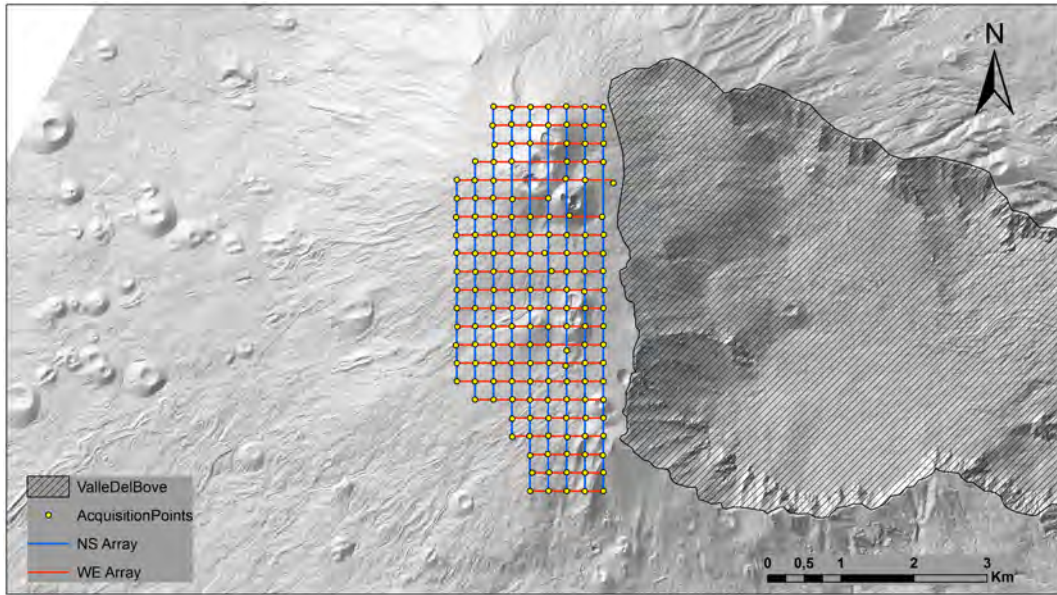


Figure 4: Digital Elevation Model of Mt. Etna as basemap. The 22 W-E arrays (red) and 9 S-N arrays (blue) are imposed on the topography.

113 3.2. Seismic data collection experiment

114 To reach the 161 points created during the setup phase we used a tablet PC with a CPU
 115 Quad-core 1.4 GHz Cortex-A9, 2GB of RAM, and an internal GPS. This was supported by
 116 an external GPS antenna equipped with a chipset SiRF Star III, a 20 channels receiver, able
 117 to process signals from all the visible satellites GPS and WAAS, a frequency of 1575,42 MHz
 118 and a TTFF (Time to First Fix) lower than 1 second. We were able to see in real time our
 119 position in the field thanks to the connection to the WebGIS and/or the map available on
 120 the tablet PC. With respect to the set of measurement points, we obtained a precision of:

- 121 • 66% in positioning inside the buffer radius of 5 meters;
- 122 • 84% in positioning inside the buffer radius of 10 meters;
- 123 • 91% in positioning inside the buffer radius of 15 meters.

124 This means that just 9% of the measurements were located outside the buffer radius of 15
 125 meters (Fig. 5).

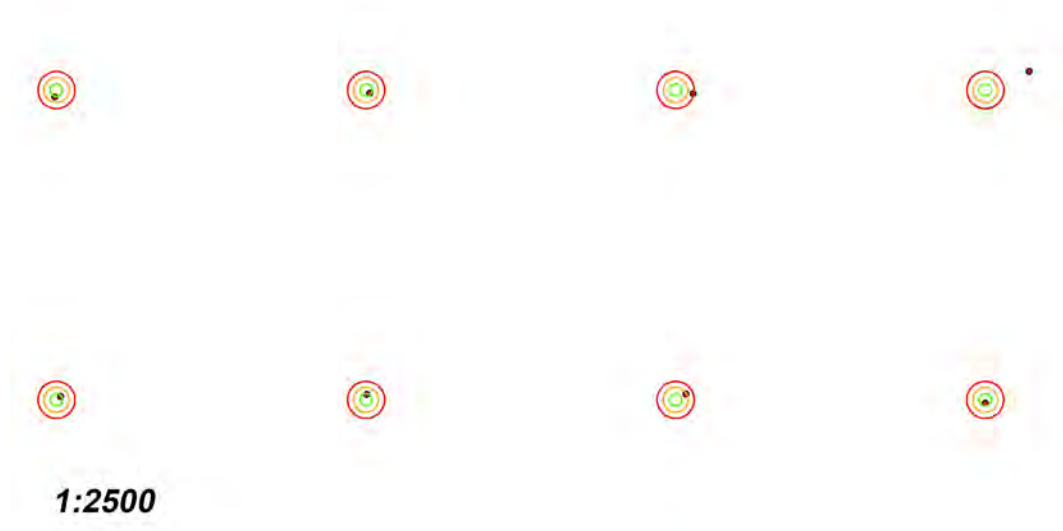


Figure 5: The example area shows the buffer radius of 5 meters (in green), 10 meters (in orange) and 15 meters (in red). The red dots indicate the acquisition points.

126 The seismic instrument, a compact seismometer (24 bit digital) equipped with 3 accelero-
 127 metric channels and 3 velocimetric channels with adaptable dynamic range, was suitable for
 128 seismic ambient noise recordings (up to 1.5 mm/s) due to its high sensitivity and a frequency
 129 operating range between 0.1 and 1024 Hz on all channels. It was located at each of the 161
 130 measurement points. The positioning on the ground was done considering several factors:

- 131 – Coupling with the soil, we used the ash of the volcano to smooth the impedance
 132 contrast;
- 133 – Setting horizontally with the spirit level;
- 134 – Orienting to the North.

135 The acquisition duration at each of the 161 points was 20 minutes with a 128 Hz sampling
 136 rate, meaning that signals are investigated up to a frequency of 64 Hz, i.e., half of the
 137 sampling rate of the discrete signal processing system. The period of acquisition is May
 138 11- June 11 2014. The volcanic tremor in this period can be considered stationary, with a

139 variation of 13.7% in amplitude and 2.6% in frequency (G. Di Grazia, INGV-Osservatorio
140 Etneo, personal communication).

141 4. Methods and Data Processing

142 The Horizontal to Vertical Spectral Ratio (HVSR) technique, applied first by [Nogoshi](#)
143 [and Igarashi \[1970, 1971\]](#) and also known as “Nakamura’s method” [[Nakamura, 1989](#)], states
144 that the ratio between the horizontal and vertical spectral amplitudes of the natural mi-
145 crotremors (volcanic noise in this case) eliminates the seismometer transfer-function and
146 gives the amplification produced by a surface layer at the recorded site. Even if, as of today,
147 there are several studies that have applied the method to different scopes, one of the main
148 hypothesis regarding the subsurface (geology) is that the fundamental frequency is linked to
149 the depth and seismic velocity of a layer topping a relevant acoustic impedance contrast [[La-](#)
150 [chetl and Bard, 1994](#)]. The fundamental resonance frequency F_0 for a continuous stratified
151 layer is given by the equation:

$$F_0 = V_s/4H$$

152 where V_s is the shear wave velocity and “4H” is 4 times the depth of the contrast. [Lermo](#)
153 [and Chávez-García \[1994\]](#) and [Dravinski et al. \[1996\]](#) state that the method is valid in the
154 assumption that microtremors are composed by surface (Rayleigh) waves, which propagate
155 inside a surface layer over an infinite half-space. Nevertheless, data-driven studies generally
156 agree that the HVSR mainly reveal the fundamental (resonant) frequency of the shallow
157 structure beneath the investigation site [[Field and Jacob, 1995](#); [Lachet et al., 1996](#); [Seekins](#)
158 [et al., 1996](#); [Coutel and Mora, 1998](#)].

159 The extension of the method to a stratified multi-layered system was given by [Konno and](#)
160 [Ohmachi \[1998\]](#). Since then, the method has been considered reliable when the structures
161 beneath the investigation site can be approximated by a 1-D model. Nevertheless, a recent
162 study of lateral heterogeneity in small alluvial valleys made by [Chávez-García and Kang](#)
163 [\[2014\]](#) proves that the method reasonably shows the natural vibration frequency of complex
164 2D structures, at least when there is a high impedance contrast between a sedimentary layer

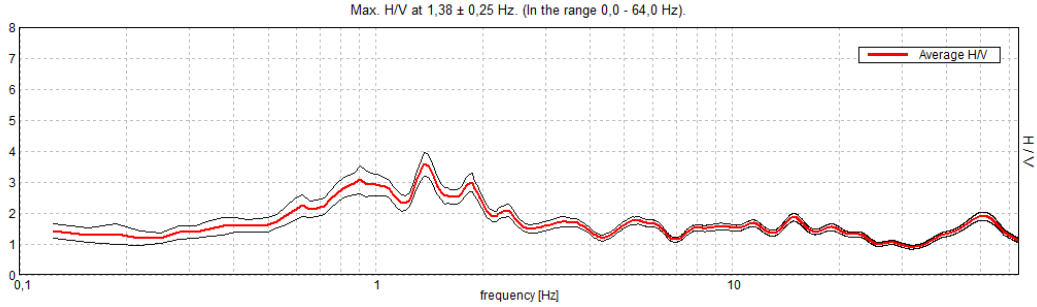


Figure 6: Sample of H/V ratios as a function of frequency. The red and black solid lines indicate the H/V mean value and standard deviation, respectively.

165 and a bedrock. The method has already been applied to a volcanic environment (Arenal
 166 volcano, Costa Rica) by [Mora et al. \[2001\]](#). These authors show that reliable HVSRs can
 167 be obtained from different types of volcanic media, with lateral heterogeneity in the shallow
 168 structures producing large variations along the array. The main result is that local amplifica-
 169 tions observed in the spectral bands, corresponding to different peaks in the spectral ratios,
 170 are related to shallow geological structures. In their interpretation, the lack of pronounced
 171 discontinuity between a shallow soft depositional layer and a deep competent materials is
 172 marked by very low amplitudes. [Galgaro et al. \[2014\]](#) demonstrate that the HVSR peak
 173 broadness can be related to thermal properties. In addition, low seismic frequencies (3
 174 Hz) highlight shallow structures in a volcanic environment such as deposited debris flows
 175 [[De Siena et al., 2016](#)], at least when using alternative stochastic (coda) waves. With the
 176 HVSR, just a few minutes of acquisition of seismo-volcanic noise are sufficient to stabilize
 177 results. Information achievable from the resonant frequencies is then precisely linked to
 178 location with the implementation of the GIS approach, thus increasing spatial correlation
 179 between the measurements and local geology.

180 In the acquisition of the relative H/V spectral ratios (Fig. 6) from volcanic noise ampli-
 181 tudes we took into account the position of the 161 data points as well as the difficulties and
 182 restrictions of Nakamura's method. We use the standard inversion method that assumes a
 183 velocity-depth function, to compute the resonant frequency F_0 [[Ibs-von Seht and Wohlen-
 184 berg, 1999](#); [Amorosi et al., 2008](#)]. This function is calculated using an average shear-wave

185 velocity of 1250 m/s at the base of the volcanic edifice, derived from [Alparone et al. \[2012\]](#)
186 and assuming a velocity of 450 m/s in the shallowest layers. This last value is obtained
187 by the seismic refraction experiment of [Cassinis et al. \[1969\]](#). Differently from geotechnical
188 applications (e.g [Amorosi et al. \[2008\]](#)) our objective is to compare H/V functions with vol-
189 canological maps, not to obtain the exact stratigraphy at each point. Hence, we perform a
190 high-resolution spatial analysis based on point interpolation with an approach similar to the
191 one devised and tested by [Almendros et al. \[2004\]](#). At each measurement point laying on
192 the lines created during the set up of the GIS workspace we obtain the related “ratiograms”.
193 These HVSR functions are shown as a 2-dimensional contour plot versus frequency and time
194 (See Supplementary Fig. 1) and were created to check for the presence of transient signals,
195 which invalidate the assumption of noise stationarity. After removal of these transients we
196 interpolate the ratiograms on the same line in space. The resulting HVSRs functions are
197 displayed in a 2-dimensional contour plot versus depth (displayed in meters above sea level)
198 and distance (in meters - Fig. S2).

199 We obtain 31 vertical cross-sections, 9 S-N oriented with a length span between 2750m
200 and 5250m (Fig. S3 and S4), and 22 with a W-E orientation (Figs. S5, S6, S7, S8 and
201 S9), with a minimum length of 975 m and a maximum length of 2135 m. The depth spans
202 between 1400 m and 3200 m a.s.l. while resolution is approximately 200 m. The H/V ratios
203 are highlighted using contour lines in a range between 1 and 4.5.

204 Doing a spline interpolation between the points obtained from the intersection of a hor-
205 izontal plane and the H/V ratio contour lines of the vertical cross-section, we additionally
206 obtain 9 horizontal cross-sections in a depth span between 1600 m and 3200 m a.s.l. (exclud-
207 ing 1400 m a.s.l. where we had a limited number of intersection points). The gap between
208 layers is 200 m. From the contour lines of the horizontal cross-section we extrapolated
209 several polygons for the different value of the H/V ratio. To correlate the distribution of
210 these horizontal cross-sections with the volcano-tectonic setting we took into consideration:
211 (1) the main alignment of the polygons and (2) the main angle direction outlined by the
212 segments constituting the polygons. From the HVSR contour line map we select polygons
213 defined by the first closed loop to avoid any misinterpretation due the spatial interpolation;

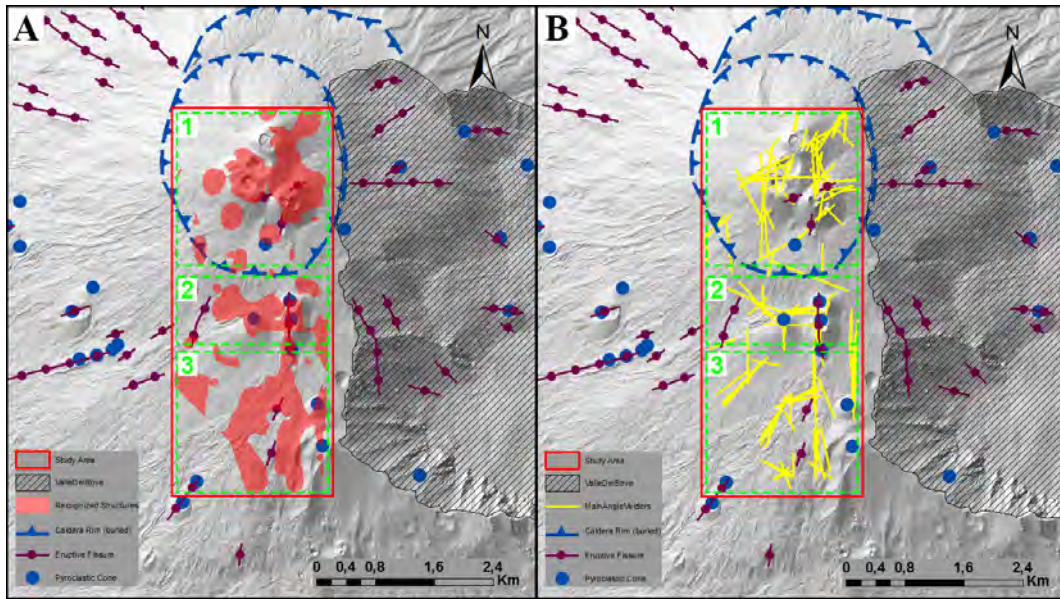


Figure 7: A: Map view of the polygons with H/V ratio equal and higher than 3.5. B: Distribution of the vectors lines obtained from the polygons' main angle. The eruptive fissures, pyroclastic cones and caldera rim are obtained from the “Volcano-Tectonic Map of Etna Volcano” [Azzaro et al., 2012]. **The green boxes indicate the three main clusters discussed in the text.**

214 this value describes polygons corresponding a value equal and higher than 3.5 (Fig. 7A). The
 215 main angle direction of the polygons was calculated using the GIS tool “CalculatePolygon-
 216 MainAngle”. This calculates the dominant angles, i.e., the orientations of segments forming
 217 the input polygon features that are measured most frequently. We then plot the segments
 218 as yellow oriented vectors on the volcano-tectonic map of Etna made by Azzaro et al. [2012],
 219 including the eruptive fissures, the pyroclastic cones, and the caldera rim (Fig. 7B). Keep-
 220 ing into consideration the sum of the length of the vectors with the same orientation we
 221 observe: (1) absolute vector maxima along the N-S direction; (2) two relative maxima along
 222 the NE-SW and E-W directions. The NW-SE trend is the least represented.

223 After importing the polygons delineated by the contour line with H/V ratio equal and
 224 higher than 3.5 in the 3D GIS environment, we gave them a vertical extrusion of 200 m,
 225 filling the gap between layers. Fig. 8 shows a 3D image of the real geographic position of
 226 the recognized structures from a pitch angle of 30° (Fig. 8).

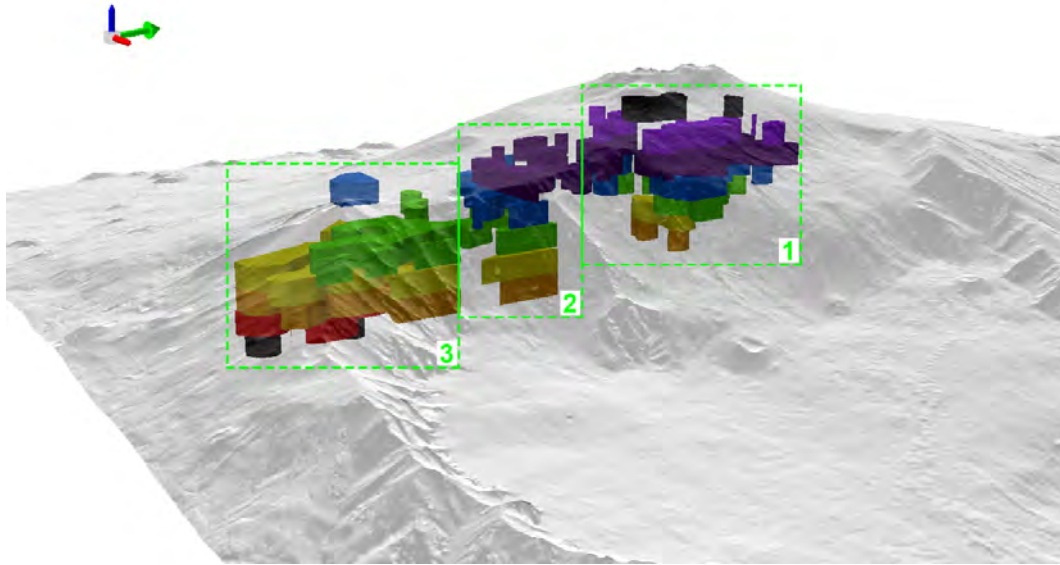


Figure 8: 3D view from a pitch angle of 30° of the recognized clusters. The green arrow on the upper left corner shows the North. The extruded polygons have a thickness of 200 m. The colour legend is (from bottom to top): black, red, orange, yellow, green, blue, indigo, violet and black and indicate depths from 1600 m to 3200 m. a.s.l.. **The green boxes indicate the three main clusters discussed in the text.**

227 5. Results and Discussions

228 The results reveal three main anomalies: two are located South of the caldera rim (**Fig.**
 229 **7A2-3**) while the third is inside it (**Fig. 7A1**). Vectors orientations South of the old caldera
 230 rim of the Ellittico volcano follow the N-S and NE-SW trends (**Fig. 7B2-3**), differing from
 231 those inside the caldera (**Fig. 7B1**). These trends are related to fractures with the same
 232 orientation, considered as preferential way for the magma uprise [Acocella and Neri, 2003].
 233 The same orientations are drawn on the INGV tectonic map of Azzaro et al. [2012] by
 234 pyroclastic cones and eruptive fissures. A similar spatial correlation is visible between all
 235 the fissures post 1900 described by Neri et al. [2011] and both the polygon map (Fig. 9A)
 236 and the vectors map (Fig. 9B).

237 Inside the rim, vectors mainly highlight the W-E and NW-SE trends, showing clear
 238 correlation with eruptive fissures directions on the north-western and eastern sides of the
 239 volcano (Valle Del Bove - Fig. 10).

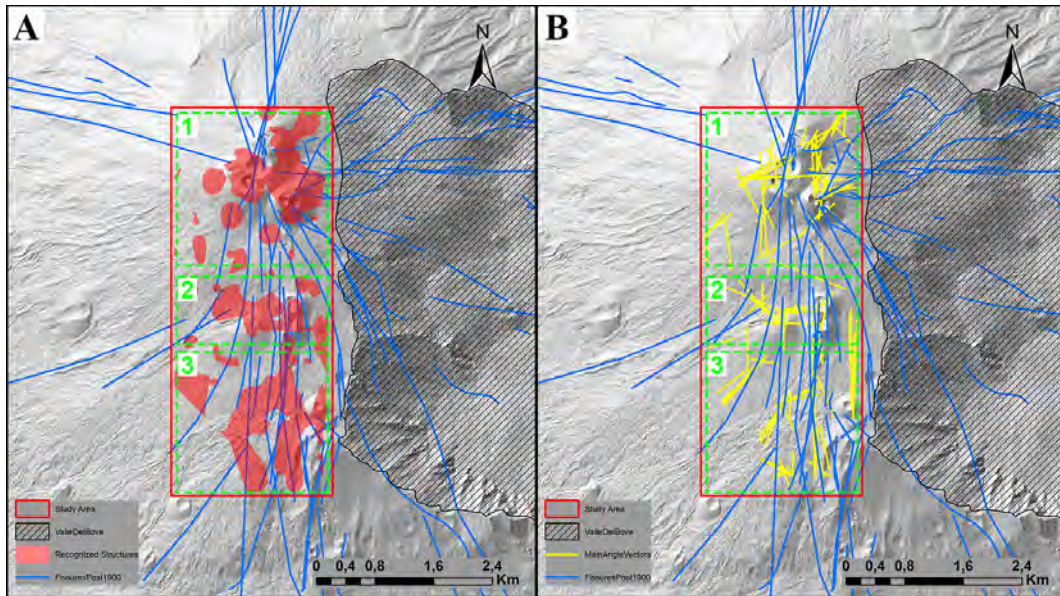


Figure 9: Correlation between the eruptive fissure post 1900 and (A) the polygon map and (B) the vectors lines obtained from the polygons' main angle. **The green boxes indicate the three main clusters discussed in the text.**

240 The southernmost and northernmost high-H/V structures could be associated with pre-
 241 existing volcanic centres. They are in reasonable spatial correlation with a cooled pathway
 242 of magma (i.e. a system of dikes) at Cuvigghiuni [Branca et al., 2004] (**box number 3 in**
 243 **Figs. 7,8 and 9**) and in the Stratovolcano Supersynthem (i.e. the centers of the Ellittico
 244 and Mongibello [Branca et al., 2011a]) inside the Ellittico caldera (**box number 1 in Figs.**
 245 **7,8 and 9**). Referring to the cross-section of the Geological Map of Etna [Branca et al.,
 246 2011b], the recognized structures intersect the Zappini, Concazze and Il Piano Synthems.
 247 The central anomaly (**box number 2 in Figs. 7,8 and 9**), however, does not correspond
 248 to any known pre-existing structures. Considering that the Cuvigghiuni center (**South**) is
 249 dated between 79.6 ± 4.2 ka and 65.3 ± 4.4 ka ago and the Stratovolcano centers (**North**)
 250 are dated between 56.6 ± 15.4 ka and 15 ka ago [De Beni et al., 2011] the central connecting
 251 structure could be an intermediate volcanic center not dated yet, and with no evidence
 252 on topography (Fig. 8-2). The high-H/V structures, however, are also in strong spatial
 253 correlation with the results of recent studies carried out using remote sensing analysis (Fig.

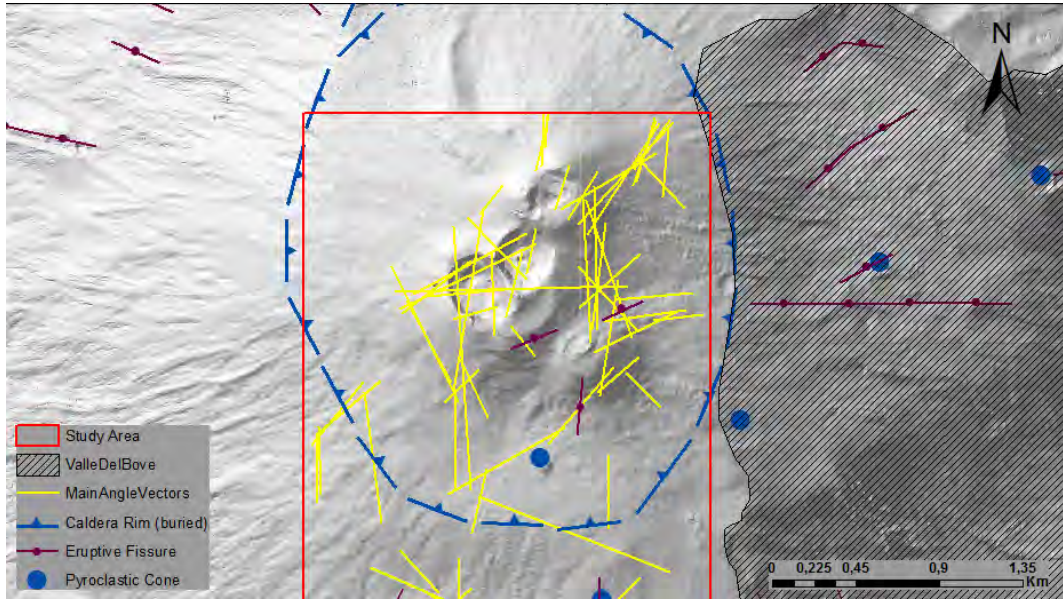


Figure 10: Detail of the vectors orientation inside the Ellittico caldera rim.

254 11) and discussed in the following sections.

255 5.1. Monte Frumento Supino and Montagnola Clusters

256 The structures comprised in the southern and intermediate clusters are located between
 257 1600 m a.s.l. and 2800 m a.s.l.. The anomalies retrieved between depths of 1600 m and 1800
 258 m a.s.l. have the same orientation of the eruptive fissures and follow the eruptive vents in
 259 the southern part of the study area (see detail in Fig. 12). Using seismic and geodetic data,
 260 Acocella and Neri [2003] highlight the dike that produced both the 2001 eruption at Piano
 261 del Lago and the deformation beneath Montagnola, producing uplift along a N-S trend.
 262 Resonant anomalies between 2000 m and 2400 m a.s.l. (thus comprising the depth range of
 263 the dike) show a similar N-S trend, (D1, Fig. 13), generally bordering the inferred location
 264 of the dike. Due to their spatial relation with eruptive fissures, we infer that the solidified
 265 dike acts as a quasi-vertical barrier for seismic noise, constraining the anomaly under areas
 266 of higher fracturing and temperature.

267 The correspondence between the recognized structures and the elements of the volcano-
 268 tectonic map is even more evident for the intermediate cluster (Fig. 13). The resonant
 269 structures between 2600 m and 2800 m a.s.l. are mainly located beneath both Monte

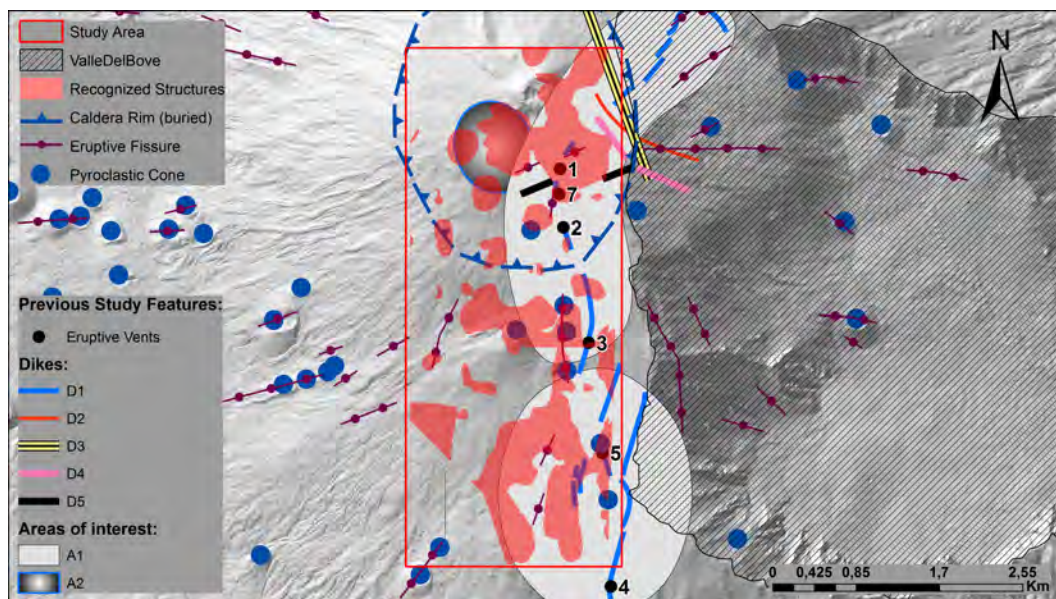


Figure 11: Comparison between the recognized structures and previous studies. In detail, the eruptive vents were described by [Acocella and Neri \[2003\]](#); [Behncke and Neri \[2003\]](#). dikes: D1 - [[Acocella and Neri, 2003](#)], D2 and D3 - [[Aloisi et al., 2009](#)], D4 - [[Bonforte et al., 2013](#)], D5 - [[Bonforte and Guglielmino, 2015](#)]. A1 marks the deformation area highlighted by [[Acocella and Neri, 2003](#)] while A2 is the Hypocenter location described by [[Saccorotti et al., 2007](#)].

270 Frumento Supino and the eruptive vents opened at about 2790 m elevation during the
 271 17 July-8 August 2001 eruption [[Behncke and Neri, 2003](#)]. The anomalies could also shape
 272 the dike's intrusion that generated the October 26 2002 eruption in the same area [[Aloisi
 273 et al., 2003](#)].

274 5.2. Crater Cluster

275 The resonant structures in the northern cluster, inside the crater, confirm the existence of
 276 a system of dikes in the area close to the SE craters (SEC) and the New SE Crater (NSEC),
 277 where our model shows resonant structures between 2400 m and 3200 m a.s.l.. This system
 278 formed the eruptive fissures and the vents 1, 2 and 7 described by [Acocella and Neri \[2003\]](#)
 279 during the 2001 eruption, which coincide with the F1, F2 and F3 vents described by [Behncke
 280 and Neri \[2003\]](#) (Fig. 14). The above-mentioned structures also depict the intrusion that
 281 caused the eruptive fissures delineated by [Bonaccorso et al. \[2011\]](#) and [Bonforte et al. \[2013\]](#)

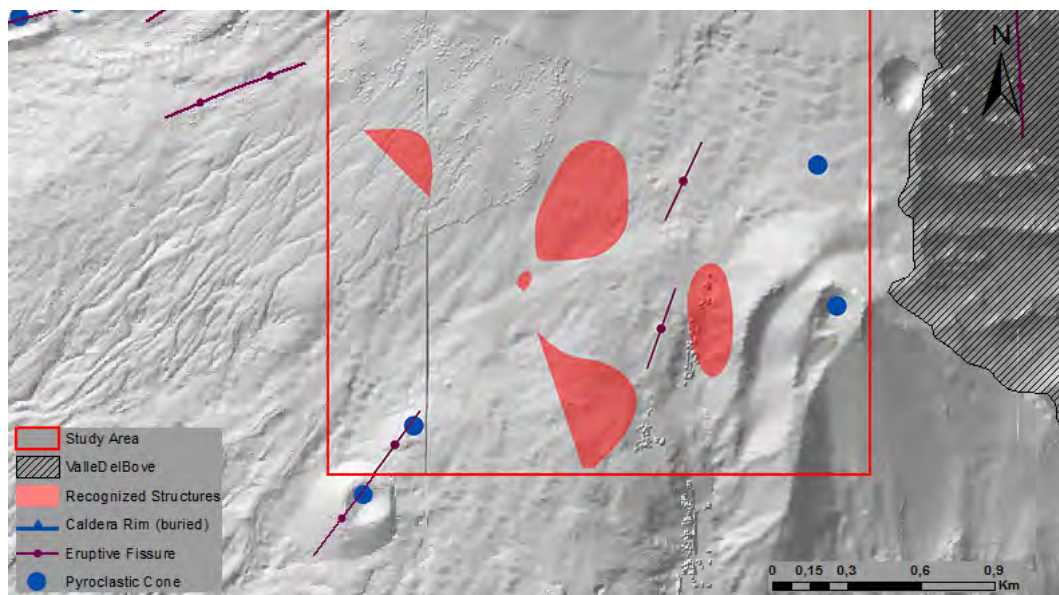


Figure 12: Comparison between the recognized structures at depth of 1600 m and 1800 m a.s.l. and the elements of the volcano-tectonic map in the southern part of the study area.

282 during the 2008-2009 eruption and [Bonforte and Guglielmino \[2015\]](#) during the 2014 eruption
 283 (Fig. 14). Considering their orientation, from 2600 m a.s.l. to the surface, the
 284 model confirm (1) the hypothesis of the influence of flank spreading on the
 285 summit crater area, considering the angles N-S oriented between SE and NE
 286 craters, and (2) the role of the upper NE Rift in radial magma intrusion (from
 287 NEC), considering the NE-SW angle orientation at North of the NEC (Fig. 10
 288 and 14) [[Bonforte et al., 2007](#)]. Finally, in the area of Voragine (VOR) and Bocca
 289 Nuova (BN), both parts of the central crater, the model reconstructs the body that causes
 290 the seismicity analyzed by [Saccorotti et al. \[2007\]](#) (Fig. 14).

291 We conclude that our results reconstruct the shallowest feeding systems of Etna. In the
 292 supplementary materials we provide a dynamic 3D visualization of the model to help in
 293 the understanding of the spatial correlation of the model with the above-discussed volcano-
 294 tectonic structures.

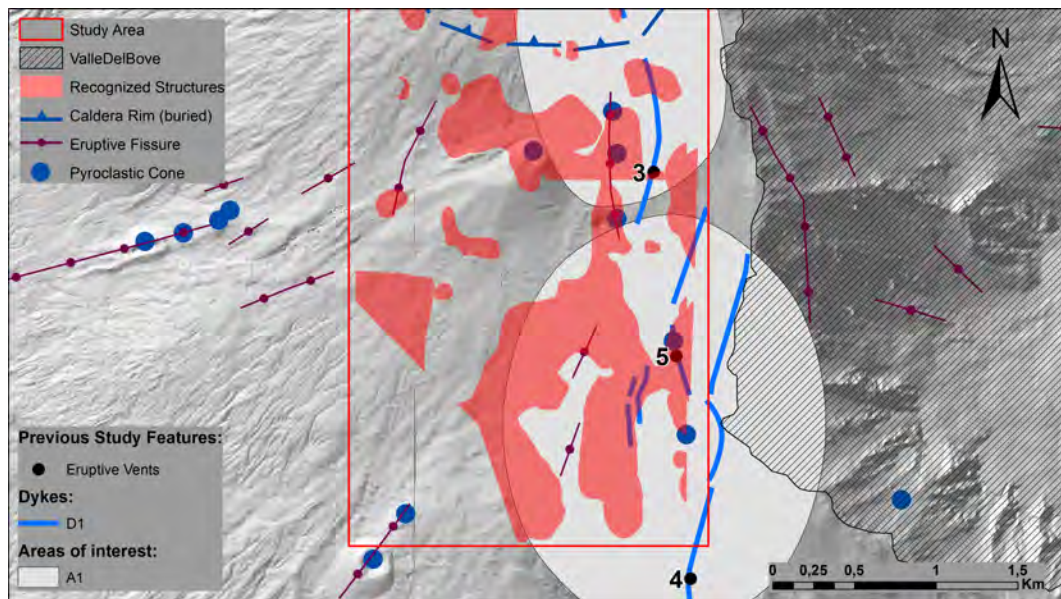


Figure 13: Comparison between the recognized structures in the central and southern clusters and previous studies. The eruptive vents were described by [Acocella and Neri \[2003\]](#); [Behncke and Neri \[2003\]](#) while the dike D1 and the deformation area A1 were described by [Acocella and Neri \[2003\]](#).

295 6. Conclusion

296 A joint seismic and GIS experiment targeting the resonant structures located between
 297 1600 and 3200 m a.s.l. at Mt. Etna volcano is carried out using a dense seismic network with
 298 a node spacing of 250 m and using the Horizontal-to-Vertical-Spectral-Ratio method. The
 299 GIS environment provides spatial interpolation between radiograms, allows a more reliable
 300 interpretation of the results by the creation of 2D and 3D models of structures with high
 301 H/V ratios, and precisely connects the results in space with remote sensing studies and
 302 geological knowledge. This new methodology increases the level of detail on subsurface
 303 shallow structures with a simple and fast analysis. The results confirm previous structural
 304 models of the volcano and present important correlations with its recent eruptive and magma
 305 dynamics.

306 Both the methodology and the technology applied have proved to be suitable to (1)
 307 the reconstruction of cooled volumes interested by magmatic intrusions in the shallowest
 308 portion of the volcano and (2) the understanding of the volcano past and recent dynam-

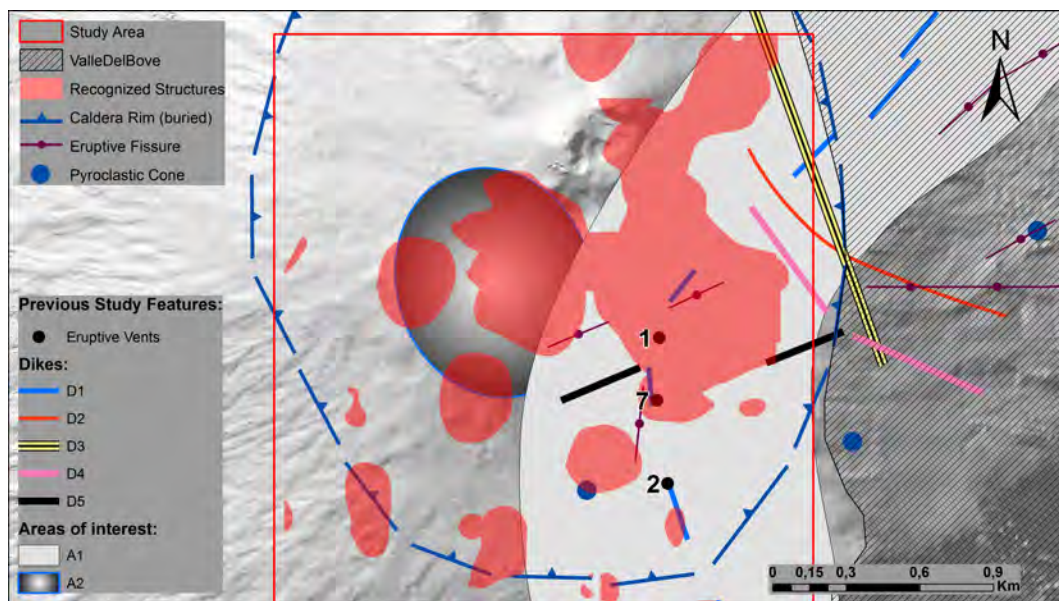


Figure 14: Comparison between the recognized structures in the northern cluster and previous studies. The eruptive vents were described by [Acocella and Neri \[2003\]](#); [Behncke and Neri \[2003\]](#). Regarding the dike: D1: [[Acocella and Neri, 2003](#)], D2 and D3: [[Aloisi et al., 2009](#)], D4: [[Bonforte et al., 2013](#)], D5: [[Bonforte and Guglielmino, 2015](#)]. The A1 indicates the deformation area highlighted from [[Acocella and Neri, 2003](#)] while the A2 is the area where hypocenters are located by [Saccorotti et al. \[2007\]](#).

309 ics. Repeating the survey in a different time period is a necessary step to (1) confirm the
 310 validity of the method; (2) test the method as a dynamic marker of the behaviour of the
 311 feeding systems before and after an eruption; (3) develop the platform into a quasi-real time
 312 analysis visualization tool for resonating, intrusive, erupting structures. Recent technologi-
 313 cal advancements in sensor miniaturization are crucial to implement the platform, reducing
 314 risks for operators as well as instrumentation costs.

315 7. Acknowledgements

316 We are very grateful to Professor G. Patanè for the inspiration and financial support; S.
 317 La Delfa for assistance during the analysis. We also thank the Parco dell'Etna Staff who
 318 ensure the permission and regular support above the volcano. We would like to thank G.
 319 Vaccino and F. Zuccarello for the support during the field trip. Two anonymous reviewers
 320 provided comments that improved both the interpretation of the results and the clarity

321 of the analyses. Finally, we are grateful to S. Castellaro, M. Neri, and G. Di Grazia for
322 providing important methodological explanations, the DEM, and data of volcanic tremor
323 during the period.

References

- Valerio Acocella and Marco Neri. What makes flank eruptions? The 2001 Etna eruption and its possible triggering mechanisms. *Bulletin of Volcanology*, 65(7):517–529, 2003.
- Javier Almendros, Francisco Luzón, and Antonio Posadas. Microtremor analyses at Teide Volcano (Canary Islands, Spain): assessment of natural frequencies of vibration using time-dependent horizontal-to-vertical spectral ratios. *Geodetic and Geophysical Effects Associated with Seismic and Volcanic Hazards*, pages 1579–1596, 2004.
- M Aloisi, A Bonaccorso, S Gambino, M Mattia, and G Puglisi. Etna 2002 eruption imaged from continuous tilt and GPS data. *Geophysical research letters*, 30(23), 2003.
- M Aloisi, A Bonaccorso, F Cannavò, S Gambino, M Mattia, G Puglisi, and E Boschi. A new dyke intrusion style for the Mount Etna May 2008 eruption modelled through continuous tilt and GPS data. *Terra Nova*, 21(4):316–321, 2009.
- Salvatore Alparone, Graziella Barberi, Ornella Cocina, Elisabetta Giampiccolo, Carla Musumeci, and Domenico Patanè. Intrusive mechanism of the 2008–2009 Mt. Etna eruption: Constraints by tomographic images and stress tensor analysis. *Journal of volcanology and geothermal research*, 229:50–63, 2012.
- A Amorosi, S Castellaro, and F Mulargia. Single-Station Passive Seismic Stratigraphy: an inexpensive tool for quick subsurface investigations. *GeoActa*, 7(10), 2008.
- Raffaele Azzaro, Stefano Branca, Klaus Gwinner, and Mauro Coltelli. The volcano-tectonic map of Etna volcano, 1: 100.000 scale: an integrated approach based on a morphotectonic analysis from high-resolution DEM constrained by geologic, active faulting and seismotectonic data. *Italian journal of geosciences*, 131(1):153–170, 2012.
- Giovanni Barreca, Alessandro Bonforte, and Marco Neri. A pilot GIS database of active faults of Mt. Etna (Sicily): A tool for integrated hazard evaluation. *Journal of volcanology and geothermal research*, 251:170–186, 2013.
- Boris Behncke and Marco Neri. The July–August 2001 eruption of Mt. Etna (Sicily). *Bulletin of Volcanology*, 65(7):461–476, 2003.
- Marina Bisson, Claudia Spinetti, Marco Neri, and Alessandro Bonforte. Mt. Etna volcano high-resolution topography: airborne LiDAR modelling validated by GPS data. *International Journal of Digital Earth*, 9(7):710–732, 2016.

- Alessandro Bonaccorso, Alessandro Bonforte, Sonia Calvari, Ciro Del Negro, Giuseppe Di Grazia, Gaetana Ganci, Marco Neri, Anna Vicari, and Enzo Boschi. The initial phases of the 2008–2009 Mount Etna eruption: A multidisciplinary approach for hazard assessment. *Journal of Geophysical Research: Solid Earth*, 116(B3), 2011.
- Alessandro Bonforte and Francesco Guglielmino. Very shallow dyke intrusion and potential slope failure imaged by ground deformation: The 28 December 2014 eruption on Mount Etna. *Geophysical Research Letters*, 42(8):2727–2733, 2015.
- Alessandro Bonforte, Daniele Carbone, Filippo Greco, and Mimmo Palano. Intrusive mechanism of the 2002 NE-rift eruption at Mt Etna (Italy) modelled using GPS and gravity data. *Geophysical Journal International*, 169(1):339–347, 2007.
- Alessandro Bonforte, Francesco Guglielmino, and Giuseppe Puglisi. Interaction between magma intrusion and flank dynamics at Mt. Etna in 2008, imaged by integrated dense GPS and DInSAR data. *Geochemistry, Geophysics, Geosystems*, 14(8):2818–2835, 2013.
- Stefano Branca, Mauro Coltelli, and Gianluca Groppelli. Geological evolution of Etna volcano. *Mt. Etna: volcano laboratory*, pages 49–63, 2004.
- Stefano Branca, Mauro Coltelli, and Gianluca Groppelli. Geological evolution of a complex basaltic strato-volcano: Mount Etna, Italy. *Italian Journal of Geosciences*, 130(3):306–317, 2011a.
- Stefano Branca, Mauro Coltelli, Gianluca Groppelli, and Fabio Lentini. Geological map of Etna volcano, 1:50,000 scale. *Italian Journal of Geosciences*, 130(3):265–291, 2011b.
- Daniele Carbone, Dominique Gibert, Jacques Marteau, Michel Diamant, Luciano Zuccarello, and Emmanuelle Galichet. An experiment of muon radiography at Mt Etna (Italy). *Geophysical Journal International*, 196(2):633–643, 2014.
- C Cardaci, M Coviello, G Lombardo, G Patanè, and R Scarpa. Seismic tomography of Etna volcano. *Journal of volcanology and geothermal research*, 56(4):357–368, 1993.
- R Cassinis, I Finetti, P Giese, C Morelli, L Steinmetz, and O Vecchia. Deep seismic refraction research on Sicily. *Boll. Geof. Teor. Appl*, 11(43/44):140–160, 1969.
- Francisco J Chávez-García and Tae-Seob Kang. Lateral heterogeneities and microtremors: limitations of HVSR and SPAC based studies for site response. *Engineering Geology*, 174:1–10, 2014.
- Fabien Coutil and Peter Mora. Simulation-based comparison of four site-response estimation techniques. *Bulletin of the Seismological Society of America*, 88(1):30–42, 1998.
- Gilda Currenti, Rosalba Napoli, and Ciro Del Negro. Toward a realistic deformation model of the 2008 magmatic intrusion at Etna from combined DInSAR and GPS observations. *Earth and Planetary Science Letters*, 312(1):22–27, 2011.
- Emanuela De Beni, Stefano Branca, Mauro Coltelli, Gianluca Groppelli, and Jan R Wijbrans. 40Ar/39Ar

- isotopic dating of Etna volcanic succession. *Italian Journal of Geosciences*, 130(3):292–305, 2011.
- P. De Gori, C. Chiarabba, and D. Patanè. Qp structure of Mount Etna: Constraints for the physics of the plumbing system. *Journal of Geophysical Research*, 110(B05303):doi:10.1029/2003JB002875, 1999.
- G De Luca, L Filippi, G Patanè, R Scarpa, and S Vinciguerra. Three-dimensional velocity structure and seismicity of Mt. Etna volcano, Italy. *Journal of volcanology and geothermal research*, 79(1):123–138, 1997.
- L. De Siena, E. Del Pezzo, and F. Bianco. Campi Flegrei seismic attenuation image: evidences of gas reservoirs, hydrothermal basins and feeding systems. *Journal of Geophysical Research*, 115(B0):9312–9329, 2010.
- L De Siena, C Thomas, and R Aster. Multi-scale reasonable attenuation tomography analysis (MuRAT): An imaging algorithm designed for volcanic regions. *Journal of Volcanology and Geothermal Research*, 277:22–35, 2014.
- Luca De Siena, Marie Calvet, Keira J Watson, ART Jonkers, and Christine Thomas. Seismic scattering and absorption mapping of debris flows, feeding paths, and tectonic units at Mount St. Helens volcano. *Earth and Planetary Science Letters*, 442:21–31, 2016.
- Ciro Del Negro, Annalisa Cappello, Marco Neri, Giuseppe Bilotta, Alexis Hérault, and Gaetana Ganci. Lava flow hazards at Mount Etna: constraints imposed by eruptive history and numerical simulations. *Scientific reports*, 3, 2013.
- M Dravinski, G Ding, and K-L Wen. Analysis of spectral ratios for estimating ground motion in deep basins. *Bulletin of the Seismological Society of America*, 86(3):646–654, 1996.
- Edward H Field and Klaus H Jacob. A comparison and test of various site-response estimation techniques, including three that are not reference-site dependent. *Bulletin of the seismological society of America*, 85(4):1127–1143, 1995.
- Pinde Fu and Jiulin Sun. *Web GIS: principles and applications*. Esri Press, 2010.
- Antonio Galgaro, Jacopo Boaga, and Michele Rocca. HVSR technique as tool for thermal-basin characterization: a field example in NE Italy. *Environmental Earth Sciences*, 71(10):4433–4446, 2014.
- PY Gillot, G Kieffer, and R Romano. The evolution of Mount Etna in the light of potassium-argon dating. *Acta Vulcanol*, 5:81–87, 1994.
- Zohar Gvirtzman and Amos Nur. The formation of Mount Etna as the consequence of slab rollback. *Nature*, 401(6755):782–785, 1999.
- Alfred Hirn, Alexandre Nercessian, Martine Sapin, Fabrizio Ferrucci, and Gérard Wittlinger. Seismic heterogeneity of Mt Etna: structure and activity. *Geophysical Journal International*, 105(1):139–153, 1991.
- Malte Ibs-von Seht and Jürgen Wohlenberg. Microtremor measurements used to map thickness of soft sediments. *Bulletin of the Seismological Society of America*, 89(1):250–259, 1999.

- Eric Kiser, Imma Palomeras, Alan Levander, Colin Zelt, Steven Harder, Brandon Schmandt, Steven Hansen, Kenneth Creager, and Carl Ulberg. Magma reservoirs from the upper crust to the Moho inferred from high-resolution Vp and Vs models beneath Mount St. Helens, Washington State, USA. *Geology*, 44(6): 411–414, 2016.
- Katsuaki Konno and Tatsuo Ohmachi. Ground-motion characteristics estimated from spectral ratio between horizontal and vertical components of microtremor. *Bulletin of the Seismological Society of America*, 88(1):228–241, 1998.
- I. Koulakov, D. Bindi, S. Parolai, H. Grosser, and C. Milkereit. Distribution of Seismic Velocities and Attenuation in the Crust Beneath the North Anatolian Fault (Turkey) from Local Earthquake Tomography. *Bulletin of the Seismological Society of America*, 100(1):207–224, 2010.
- Ivan Koulakov. Studying deep sources of volcanism using multiscale seismic tomography. *Journal of Volcanology and Geothermal Research*, 2013.
- Corinne Lachet, Denis Hatzfeld, Pierre-Yves Bard, Nikos Theodulidis, Christos Papaioannou, and Alekos Savvaidis. Site effects and microzonation in the city of Thessaloniki (Greece) comparison of different approaches. *Bulletin of the Seismological Society of America*, 86(6):1692–1703, 1996.
- Corinne Lachet and Pierre-Yves Bard. Numerical and Theoretical Investigations on the Possibilities and Limitations of Nakamura’s Technique. *Journal of Physics of the Earth*, 42(5):377–397, 1994.
- G Lanzafame and JC Bousquet. The Maltese escarpment and its extension from Mt. Etna to Aeolian Islands (Sicily): importance and evolution of a lithosphere discontinuity. *Acta Vulcanologica*, 9:113–120, 1997.
- J. M. Lees and G. T. Lindley. Three-dimensional Attenuation Tomography at Loma Prieta: Inverting t^* for Q . *Journal of Geophysical Research*, 99(B4):6843–6863, 1994.
- F Lentini. The geology of the Mt. Etna basement, *Mem. Soc. Geol. Ital*, 23:7–25, 1982.
- Javier Lermo and Francisco J Chávez-García. Are microtremors useful in site response evaluation? *Bulletin of the seismological society of America*, 84(5):1350–1364, 1994.
- RP Middlemiss, A Samarelli, DJ Paul, J Hough, S Rowan, and GD Hammond. Measurement of the Earth tides with a MEMS gravimeter. *Nature*, 531(7596):614–617, 2016.
- Mauricio M Mora, Philippe Lesage, Jacques Dorel, Pierre-Yves Bard, Jean-Philippe Métaixian, Guillermo E Alvarado, and Carlos Leandro. Study of seismic site effects using H/V spectral ratios at Arenal Volcano, Costa Rica. *Geophysical research letters*, 28(15):2991–2994, 2001.
- Yutaka Nakamura. A method for dynamic characteristics estimation of subsurface using microtremor on the ground surface. *Railway Technical Research Institute, Quarterly Reports*, 30(1), 1989.
- Marco Neri, Valerio Acocella, Boris Behncke, Salvatore Giammanco, Francesco Mazzarini, and Derek Rust. Structural analysis of the eruptive fissures at Mount Etna (Italy). *Annals of Geophysics*, 54(5), 2011.
- J. Neuberg and T. Pointer. Effects of volcano topography on seismic broad-band waveforms. *Geophysical*

- Journal International*, 143:239–248, 2000. doi: 10.1046/j.1365-246x.2000.00251.xs.
- M Nogoshi and T Igarashi. On the propagation characteristics of microtremors. *J. Seism. Soc. Japan*, 23: 264–280, 1970.
- M Nogoshi and T Igarashi. On the amplitude characteristics of microtremor (part 2). *Jour. Seism. Soc. Japan*, 24:26–40, 1971.
- S Parolai, P Bormann, and C Milkereit. New relationships between Vs, thickness of sediments, and resonance frequency calculated by the H/V ratio of seismic noise for the Cologne area (Germany). *Bulletin of the Seismological Society of America*, 92(6):2521–2527, 2002.
- D. Patanè, G. Barberi, O. Cocina, P. De Gori, and C. Chiarabba. Time-Resolved Seismic Tomography Detects Magma Intrusions at Mount Etna. *Science*, 313:821–823, 2006a.
- Domenico Patanè, Claudio Chiarabba, Omella Cocina, Pasquale De Gori, Milena Moretti, and Enzo Boschi. Solid Earth-135. Tomographic images and 3D earthquake locations of the seismic swarm preceding the 2001 Mt. Etna eruption: Evidence for a dyke intrusion (DOI 10.1029/2001GLO14391). *Geophysical Research Letters*, 29(10), 2002.
- Domenico Patanè, Pasquale De Gori, Claudio Chiarabba, and Alessandro Bonaccorso. Magma ascent and the pressurization of Mount Etna’s volcanic system. *Science*, 299(5615):2061–2063, 2003.
- Giuseppe Patanè, Santo La Delfa, and Jean-Claude Tanguy. Volcanism and mantle–crust evolution: the Etna case. *Earth and Planetary Science Letters*, 241(3):831–843, 2006b.
- Gilberto Saccorotti, Ivan Lokmer, Christopher J Bean, Giuseppe Di Grazia, and Domenico Patanè. Analysis of sustained long-period activity at Etna Volcano, Italy. *Journal of volcanology and geothermal research*, 160(3):340–354, 2007.
- Linda C Seekins, Leif Wennerberg, Lucia Margheriti, and Hsi-Ping Liu. Site amplification at five locations in San Francisco, California: A comparison of S waves, codas, and microtremors. *Bulletin of the Seismological Society of America*, 86(3):627–635, 1996.
- ADL Sharp, PM Davis, and F Gray. A low velocity zone beneath Mount Etna and magma storage. *Nature*, 287:587–591, 1980.
- U. Wegler. Analysis of Multiple Scattering at Vesuvius Volcano, Italy, using Data of the TomoVes active seismic experiment. *Journal of Volcanology and Geothermal Research*, 128:45–63, 2003.